Contents lists available at ScienceDirect

Materials and Design

journal homepage: http://ees.elsevier.com

Energy resolved-electrochemical impedance spectroscopy investigation of the role of Al-doped ZnO nanoparticles in electronic structure modification of polymer nanocomposite LEDs

Jakub Sevcik [a], Pavel Urbanek [a,*], David Skoda [a], Thaiskang Jamatia [a], Vojtech Nadazdy [b,c], Michal Urbanek [a], Jan Antos [a], Lukas Munster [a], Ivo Kuritka [a,*]

[a] Tomas Bata University in Zlin, Centre of Polymer Systems, Tr. Tomase Bati 5678, Zlin CZ-760 01, Czech Republic
[b] Institute of Physics, Slovak Academy of Sciences, Dubravska cesta 9, Bratislava SK-845 11, Slovak Republic
[c] Centre for Advanced Material Application, Slovak Academy of Sciences, Dubravska cesta 9, Bratislava SK-845 11, Slovak Republic

ARTICLE INFO

Article history:
Received 7 December 2020
Received in revised form 11 April 2021
Accepted 12 April 2021
Available online xxx

Keywords
Doped nanoparticles
Thin composite film
PLED

ABSTRACT

The work is focused on power efficiency and luminance of polymer light-emitting diodes (PLED) based on polymer matrix and nanoparticulate filler. As polymer matrices poly[2-methoxy-5-(2-ethylhexyloxy)-1,4-phenylenevinylene] (MEH-PPV) and poly[(9,9-di-n-octylfluorenyl-2,7-diyl)-alt-(benzo[2,1,3]thiadiazol-4,8-diyl)] (F8BT) were used. Nanofillers, aluminium-doped ZnO nanoparticles, were prepared by microwave-assisted polyol method and characterized by XRD, SEM, and TEM. Obtained nanoparticle colloids were mixed with dissolved polymer. Then, nanocomposite active layers of prepared PLEDs were spin-cast in one processing step. Specific optoelectronic and electric properties of nanocomposite materials and performance of PLED devices were investigated using UV–Vis absorption, photoluminescence, energy-resolved electrochemical impedance spectroscopy (ER-EIS), and I-V and luminance measurements. The addition of Al-doped ZnO nanoparticles improved power efficiency of diodes exhibiting an order of magnitude enhancement in electroluminescence intensity, luminance (from 1 900 to 20 700 cd/m^2 for MEH-PPV and from 4 600 to 38 000 cd/m^2 for F8BT) and had pronounced effect on opening bias voltage of final devices. In addition, two effects of nanoparticulate doping were revealed. The first, specific one, related with electronic structure of used nanoparticles. The second, non-specific, which indirectly contributes to structural ordering of the polymer matrix. Observed phenomena are related to electronic band structure affected by the addition of nanoparticles as revealed by ER-EIS.

1. Introduction

Polymer light-emitting diodes (PLEDs) achieve high brightness and efficiency and their operation lifetimes improve rapidly [1]. This is allowed due to the enormous development of solution-processable materials based on polymers. Such materials combine excellent processability, appropriate physical properties, and sufficient efficiency to prepare devices fulfilling the following features: high-luminance efficiency, full colour/large-area display, wide-viewing angle, lightweight and transparency and low power consumption [2–6]. Moreover, PLEDs open new potential applications such as wallpapers emitting light on-demand, flexible displays, easy integration into the interior of cars, home furniture, for example in kitchens and bathrooms, allowing revolutionary lighting design [7].

In general, organic and polymer materials are soft and frail and can undergo degradation when exposed to moisture and atmospheric oxygen [8]. This issue can be easily solved if rigid technologies are used and whole processes are conducted in an inert atmosphere. Finally, an encapsulation protects a device against interaction with the external environment. Despite substantial progress and improvement that has been made in this scientific field, some challenges remain. Among others, efficient charge carrier transport, electron-hole balance and recombination, and proper bandgap adjusting are the most challenging [9–11]. The working efficiency of PLED devices (the external quantum efficiency, η_{EQE}) can be described by the following equation [7]:

$$\eta_{EQE} = \gamma \bullet \eta_{S/T} \bullet q_{eff} \bullet \eta_{out} \quad (1)$$

where γ is a factor expressing whether the charges are in equilibrium; $\eta_{S/T}$ is the ratio of singlet and triplet excitons; q_{eff} is a factor representing the efficiency of excitons contributing to radiative recombination; η_{out} indicates the number of irradiative photons.

The majority of conjugated polymers applied in PLEDs are p-conductive; thus, the major carriers are the positively charged holes. The

* Corresponding authors.
E-mail addresses: urbanek@utb.cz (P. Urbanek); kuritka@utb.cz (I. Kuritka)

https://doi.org/10.1016/j.matdes.2021.109738
0264-1275/

charge carrier balance can be improved by the introduction of donor molecules, donating comonomers, and very easily by the addition of suitable nanoparticles [12,13]. If the p-conductive nanoparticles are incorporated into the polymer matrix, it is expected that the ratio of electrons and holes will shift more in favour of the positively charged holes, which can improve the mobility of holes that pertinently influence the opening voltage and also the conductivity of the entire device. On the opposite side, if the n-conductive nanoparticles are introduced into the polymer matrix, it is expected that the ratio of electrons and holes will shift more in favour of the negatively charged carriers. If the ratio of carriers is appropriately balanced, the efficiency of devices is improved, and the luminance is increased. For these reasons, nanocomposite materials consisting of conducting polymers and inorganic nanoparticles have attracted great interest and considerable research because of their high potential for optoelectronic and photovoltaic applications [14–20].

Applicable nanoparticles in electronic devices can be based on zinc oxide, which is an II-VI semiconductor with a direct bandgap of ca. 3.37 eV and a large exciton binding energy (about 60 meV). Due to these characteristics, along with high thermal stability [21], zinc oxide has already been demonstrated as a promising material for versatile applications in optoelectronic and piezoelectric devices [22].

Doping of zinc oxide with various metals provides an effective pathway for tuning its optoelectronic properties [23,24]. Due to interesting optoelectronic properties [25], aluminum-doped ZnO is widely studied for its application in optoelectronic devices [25–30]. For these purposes, the homogeneity and stability of prepared nanoparticles and their dispersibility and are considered crucial and decisive properties for the preparation of thin nanocomposite films. From this point of view, the nanoparticles synthesis method is one of the critical factors that affect the performance of final devices. It has already been reported that microwave-assisted syntheses provide well defined nanocrystalline particles [31]. For example, Hammarberg and coworkers reported MW-assisted polyol synthesis of nanocrystalline aluminium-doped ZnO nanoparticles with sizes of about 9–15 nm [32].

In previous work, we synthesised ZnO nanoparticles doped by Co and Fe atoms and studied their optoelectronic properties [33,34]. The bandgaps of the nanoparticles were successfully tailored, and their stability and homogeneity of prepared nanodispersions were achieved. It was also found to be beneficial for their utilisation in PLED devices with high performance in both studies; mainly because one technological step could be omitted and active layer with better transport properties is cast in one step.

In this paper, we present an extensive study wherein we synthesised aluminium-doped ZnO nanoparticles using the facile microwave-assisted polyol method introduced in the previous work [35]; and prepared thin nanocomposite films based on polymer matrices and doped ZnO nanoparticles. As polymer matrices, the MEH-PPV (a representative of *p*-type semiconductor polymers) and F8BT (an example of a balanced *p*- and *n*-type semiconductor *co*polymer) were used because both materials are prototypical electroluminescent conductive polymers which have been widely studied and still serve as model materials for understanding the complex behaviour [36–38]. The influence of the nanoparticles and the aluminium dopant concentration on the PLED performance were investigated. Observed strong positive effects in the PLEDs devices performance are correlated to the electronic structure of polymers, nanoparticles and polymers/nanoparticle composite layers characterised by the energy-resolved electrochemical impedance spectroscopy (ER-EIS) which was proven extremely powerful for electronic structure studies [39–41], even in the field of corrosion control [42,43], and other optical spectroscopic methods.

2. Materials and methods

2.1. Chemical compounds

Zinc acetate dihydrate ($Zn(OAc)_2{\cdot}2H_2O$, p.a., M_w = 219.51 g/mol[1]), diethylene glycol (p.a., DEG), oleic acid (p.a. M_w = 282.46 g/mol[1]), toluene (p.a.), and methanol (p.a.) were purchased from PENTA Czech Republic. Aluminum(III) acetylacetonate ($Al(III)(Acac)_3$, 99%, Mw = 324.31 g/mol[1]), and MEH-PPV - Poly[2-methoxy-5-(2-ethylhexyloxy)-1,4-phenylenevinylene] (Mw = 40 000–70 000 g/mol[1]), F8BT - Poly[(9,9-di-n-octylfluorenyl-2,7-diyl)-alt-(benzo[2,1,3]thiadiazol-4,8-diyl)] (Mw = 15 000–25 000 g/mol[1]) were obtained from Sigma-Aldrich. PEDOT:PSS (poly(3,4-ethylenedioxythiophene)polystyrene sulfonate - Clevios^{TM} P AI 4083) was supplied by Heraeus.

2.2. Synthesis of nanoparticles

The synthesis of Al-doped ZnO nanoparticles was carried out in a PTFE-lined microwave reactor ERTEC Magnum II (600 W; 2.45 GHz). A typical reaction was performed as follows. $Zn(OAc)_2{\cdot}2H_2O$ (0.721 g, 3.28 mmol) was mixed with 50 ml of diethylene glycol (DEG), and then $Al(III)(Acac)_3$ (0.119 g, 0.36 mmol) and oleic acid (0.653 g, 2.31 mmol) was added into the stirred solution. Teflon lined vessel with reaction precursors suspension was placed into the microwave reactor and tightly closed. Then the microwave power (100%) was applied for 15 min, and the reaction mixture was heated up to 250 °C. In the Supplementary Info, see the MW record for details (Fig. S1). When the reaction mixture was cooled down to reaction temperature, the product was separated by centrifugation and washed with methanol. The resulting white or white-yellowish precipitate (0.296 g) was dried in an oven at 80 °C.

2.3. Characterisation of nanoparticles

The UV–Vis measurements were performed on a Perkin-Elmer Lambda 1050. The optical bandgaps were determined using Tauc plot analysis from data sets achieved by DR-UV/VIS measurements. The powder XRD patterns were recorded on a Rigaku MiniFlex 600 diffractometer equipped with a CoKα (λ = 1.7903 Å) X-ray tube (40 kV, 15 mA). Data processing and crystal size calculations were done with Rigaku PDXL2 software. The average size of $Al_xZn_{1-x}O$ crystallites was evaluated using the Scherrer's formula, $d = K\lambda/\beta\cos\theta$, where d is the crystallite size, K is a grain shape-dependent constant (0.94), λ is the wavelength, θ is a Bragg reflection angle, and β is the full-width half-maximum (in 2θ scale). The observed line broadening was corrected to intrinsic sample broadening by instrumental function using B-spline background subtraction and Split pseudo-Voigt peak shape function. The crystallite sizes were also calculated by Williamson-Hall method using the external LaB_6 standard. Obtained size of the diffracting area was rounded to nanometer units expressing thus the estimated precision. Transmission electron microscopy was carried out on a JEOL JEM 2100 microscope operated at 200 kV (LaB_6 cathode, point resolution 2.3 Å) equipped with OLYMPUS SYS TENGRA camera (2048 × 2048 pixels). An OLYMPUS Soft Imaging Solutions software was used for the particle size distribution calculations. The sample for TEM analyses was prepared by dropping of $Al_xZn_{1-x}O$ dispersions on carbon-coated copper grids (300 mesh) and subsequently dried at 80 °C for 1 h. The SEM images and EDX analysis of calcined (400 °C) $Al_xZn_{1-x}O$ powders were recorded on a Nova NanoSEM (FEI) apparatus with a Schottky field emission electron source (0.02–30 keV) and a TLD detector at 5 kV. EDS platform Octane plus (SDD detector) by EDAX, AMETEK, Inc. was used for EDX analysis. Photoluminescence (PL) spectra of $Al_xZn_{1-x}O$ dispersions were collected at fluorescence spectrometer FLS920 from Ed-

inburgh Instruments, (excitation laser 332.2 nm; Xe lamp excitation 515 nm).

2.4. Thin film deposition and device preparation

The polymers (F8BT and MEH-PPV; 10 mg in all cases) were dissolved in 3.5 ml of $Al_xZn_{1-x}O$ nanodispersion containing 10 mg of nanoparticle powder and homogenised in an ultrasonic bath. The weight ratio of polymer/$Al_xZn_{1-x}O$ in the nanocomposites were set to 1:1 in all solutions. Thin layers of polymer/$Al_xZn_{1-x}O$ nanocomposites were cast onto ITO substrates by spin coating technique as follows: 120 μl of nanocomposite solution was dropped onto the substrate spinning at the speed 1000 rpm. The duration of the spin coating process was 30 s. After deposition, the layers were dried in an inert atmosphere at 100 °C for 2 h. The thicknesses of the composite layers were measured by a profilometer with resolution 1 nm. For the sake of comparison, the layers of pure F8BT, F8BT/ZnO-NPs, MEH-PPV and MEH-PPV/ZnO-NPs respectively were deposited as well.

The PLED devices with a composite active layer consisted of polymer/$Al_xZn_{1-x}O$ were prepared in an inert (N_2) atmosphere as follows: Standard patterned ITO substrates (Ossila Ltd.) with six active pixels were used for device fabrication. PEDOT:PSS was filtered through a 0.45 μm PVDF filter before being deposited as HTL (hole transporting layer) by standard procedure. The solution of polymer/$Al_xZn_{(1-x)}O$ in toluene (100 μl) was deposited onto the HTL layer by spin coating at 1000 rpm using Laurell WS-650-MZ-23NPP followed by drying at 150 °C on a hot plate. In consequence, a magnesium cathode was sputtered by Quorum Technologies Q300TT sputter-coater. All PLED devices were encapsulated by an epoxy resin prior to removing them from the protective atmosphere. The whole process of sample preparation was carried out in a glove box JACOMEX GP Concept, keeping relative partial pressure of H_2O and O_2 below 10 ppm.

2.5. Thin-film characterisation

The thickness of the layers was measured on a profilometer Dektak XT-E (Bruker) with 1 nm resolution. The novel ER-EIS method [39], was used to map the density of states (DOS) in MEH-PPV, MEH-PPV/ZnO and MEH-PPV/$Al_xZn_{1-x}O$, F8BT, F8BT/ZnO and F8BT/$Al_xZn_{1-x}O$ nanocomposite layers. Then, the layers for this analysis were deposited onto non-patterned ITO substrates by spin coating in the glove box described above. The ER-EIS method is based on the measurement of the charge transfer resistance, R_{ct}, of a semiconductor/electrolyte interface at a frequency where the redox reactions determine the real component of the impedance. Further, the DOS function $g(E)$ in the semiconductor at the electrochemical potential $E_{F,redox} = eU$ is given in terms of R_{ct} measured at the applied voltage U as [39]

$$g\left(E_{F,redox} = eU\right) = \frac{1}{e^2 k_{et}[A] S R_{ct}} \quad (2)$$

where e is the elementary charge, k_{et} is the charge-transfer rate constant, $[A]$ is the concentration of the electrolyte redox (donor/acceptor) species in the interphase region of the solid/liquid contact, and S is the sample area. The reciprocal value of the R_{ct} resistance measured as a response to the harmonic perturbation with the amplitude dU, and an appropriate frequency provides direct information about the electronic DOS at the energy-adjusted using an external voltage.

The impedance/gain-phase analyser Solartron analytical, model 1260 was used for the ER-EIS experiment. The frequency was set to 0.5 Hz, the amplitude of AC voltage, dU, was 100 mV, and the average sweep rate of the DC voltage ramp was 10 mV s^{-1}. The measurements were performed in a glove box with protective N_2 atmosphere (oxygen and moisture below 20 ppm and 2 ppm, respectively) using a common three-electrode electrochemical cell with a volume of about 200 μl. The solution of 0.1 M TBAPF6 in acetonitrile was used as the supporting electrolyte. The potential of the working electrode with respect to the reference Ag/AgCl electrode was controlled via the potentiostat. Pt wire was used as the counter electrode. The potential recorded with respect to the reference Ag/AgCl electrode can be recalculated to the local vacuum level assuming the Ag/AgCl energy vs vacuum value of 4.66 eV.

2.6. SEM analysis of diodes

Description of experimental sample preparation and the cross-sectioned images of prepared PLED are placed in Supplementary Materials.

2.7. Characterisation of device performance

Measurement of PLED performance was performed by utilising the Source Measure Unit (SMU) XTralien X100 (Ossila Ltd.). The *J-V-L* (current–voltage-luminance) characteristics were measured simultaneously. Electroluminescence spectra and intensity of PLEDs were measured using the integrating sphere (Avantes AvaSpec 2048 fibre spectrometer) under forwarding bias 10 V powered by the SMU.

The current efficiency, *CE*, is obtained as the ratio of the luminance L_{vPLED} and the current density. L_{vPLED} is obtained by calculation from luminous intensity and area of tested PLED pixel. The method of luminance and current determination is described in Supplementary Materials in more details.

3. Results and discussion

3.1. $Al_xZn_{1-x}O$ nanoparticle syntheses and characterisation of products

Aluminium doped ZnO nanoparticles ($Al_xZn_{1-x}O$, x = 0.01, 0.05, 0.1) were prepared by microwave-assisted thermal decomposition of zinc acetate dihydrate and Al(III) acetylacetonate in diethylene glycol (DEG) with the use of oleic acid (OA) as a surfactant. The precursors and the surfactant amounts are detailed in Table 1. This method produces stable nanodispersions applicable to further PLED development [33,35].

The XRD patterns displayed in Fig. 1 show diffraction lines of pure ZnO and $Al_xZn_{1-x}O$ samples. Positions of all diffraction lines (at 2θ angles 37.04°, 40.26°, 42.29°, 55.76°, 66.69°, 74.56°, 78.98°, 80.91°, 82.38° as obtained with CoKα radiation source) identified in the diffractogram by the Miller indices of corresponding planes are in accordance with the hexagonal wurtzite phase of ZnO diffraction pattern (PDF 36–1451). Furthermore, neither phase separation of Al_2O_3 nor other diffractions related to a dopant or unreacted precursor were observed. Lattice parameters for ZnO and $Al_xZn_{1-x}O$ nanoparticles are given in Suplementary materials in Table S2.

The morphology of prepared nanoparticles was studied by transmission electron microscopy. TEM images of ZnO and AlxZn1-xO nanoparticles are displayed in Fig. 2. Observed nanoparticles are well defined. The formation of small single layer agglomerates can be ascribed to the evaporation of toluene solvent within TEM sample preparation. The average particle size of prepared nanoparticles was estimated from TEM

Table 1
The molar amounts of precursors and surfactant in reaction solutions.

Sample	n_{Zn} [mmol]	n_{Al} [mmol]	n_{OA} [mmol]
Al1ZnO	3.58	0.05	2.63
Al5ZnO	3.46	0.18	2.28
Al10ZnO	3.45	0.36	2.31
ZnO	3.67	–	2.04

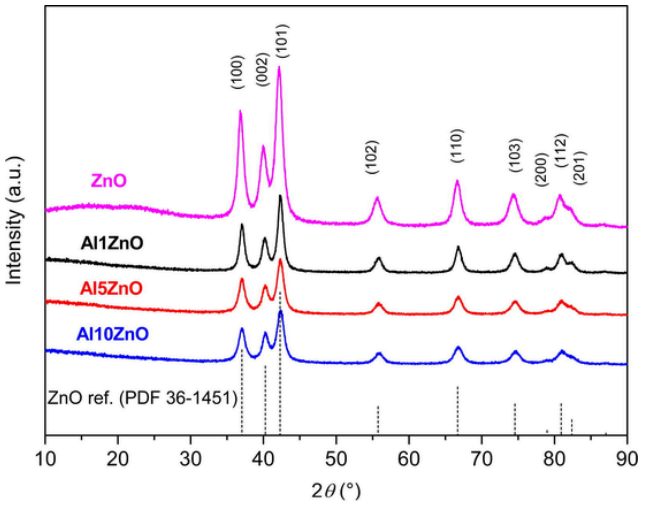

Fig. 1. Powder XRD patterns of pure ZnO and $Al_xZn_{1-x}O$ nanopowders. Observed diffractions match with the hexagonal wurtzite phase of ZnO.

images. These values are compared with the average crystallite size calculated from XRD diffraction line broadening patterns (Fig. 2) by Scherrer formula (Table 2) as described in paragraph 2.3. Moreover, the Williamson-Hall method was employed for the crystallite size calculation and obtained values are given in Table 2. The average particle size of ZnO and $Al_xZn_{1-x}O$ estimated by two methods does not show significant differences. The elemental composition of prepared nanoparticles was verified by SEM EDX and corresponded to the aluminium content calculated from the initial precursor concentrations (see Table 2, Fig. S3 and Table S2 in Supplement file).

TEM nanoparticle size is expressed with the standard deviation while the XRD calculated values are rounded to unit nm, the x^a was calculated from the ratio $n_{Al}/(n_{Al} + n_{Zn})$ in the source solution, and the x^b was experimentally verified by SEM EDX, where the at% found by EDX were used in $n_{Al}/(n_{Al} + n_{Zn})$ calculation. Crystallite size expressed by the Williamson-Hall method [44].

The UV–Vis spectra of ZnO and $Al_xZn_{1-x}O$ nanodispersions in Fig. 3**a** show strong absorption in UV region and a shift of the absorption band maximum toward lower wavelengths with increasing Al dopant content. It seems that the absorption band edge blue-shifts too. This hypsochromic shift is similar to that reported in [45] and indicates that the Al^{3+} ions are located in lattice sites substituting Zn^{2+} positions. Substitution of Zn atoms in ZnO by Al, an element belonging to the p-block of elements in the periodic table (group 13, a post-transition metal) results in the n-type doping. The optical bandgaps were estimated using Tauc plots derived from the DRUV–Vis spectra in Fig. 3b. To estimate the direct bandgap energy, the linear part of the curve was extrapolated to $[F(R).E]^2 = 0$, where the $F(R)$ represents Kubelka-Munk remission function. Compared to undoped ZnO nanoparticles

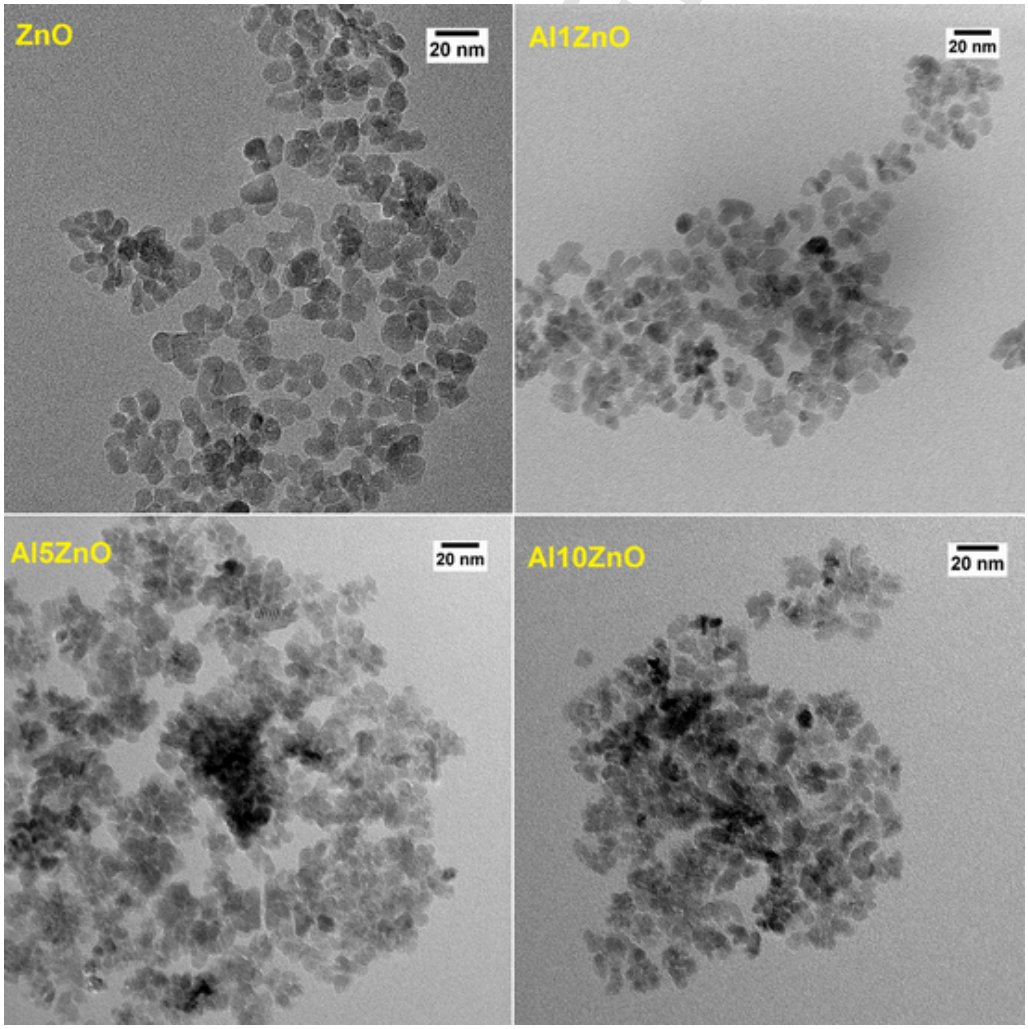

Fig. 2. TEM images of pure ZnO and $Al_xZn_{1-x}O$ nanoparticles. Scale bar: 20 nm.

Table 2
The particle size characterisation, bandgaps of $Al_xZn_{1-x}O$ products, and the Al dopant concentrations in the particles.

Sample	TEM nanoparticle size [nm]	XRD apparent crystallite size (Scherrer) [nm]	XRD crystallite size Williamson-Hall method [nm]	Al content x [at %]		Bandgap [eV]
				x^a calculated	x^b EDX	
Al1ZnO	10 ± 2	12	9.8	1.28	1.4	3.12
Al5ZnO	10 ± 2	10	7.9	5.24	5.7	3.14
Al10ZnO	9 ± 2	10	8.7	9.89	10	3.16
ZnO	8.5 ± 1.3	10	8.5	–	–	3.23

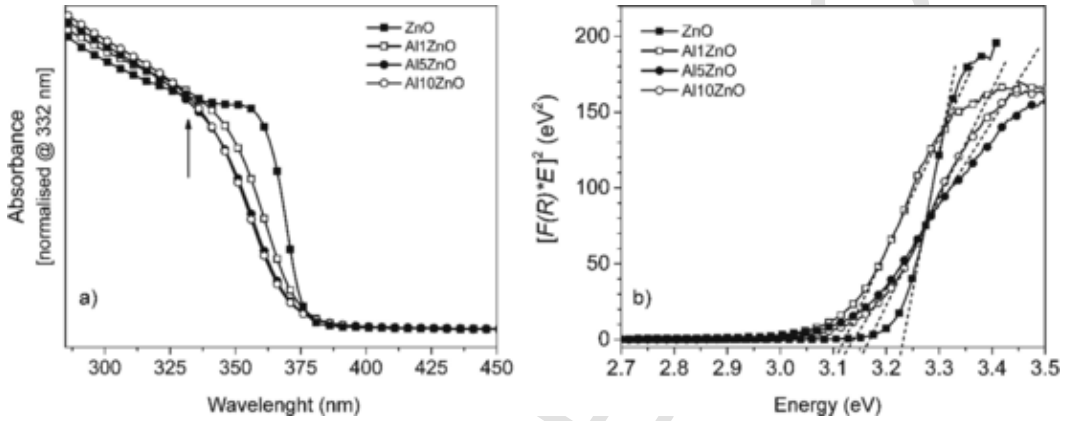

Fig. 3. a) UV–Vis spectra of ZnO and $Al_xZn_{1-x}O$ nanodispersions. The arrow marks the wavelength 332 nm. b) Plot of $[F(R)*E]^2$ versus photon energy (E) for ZnO and $Al_xZn_{1-x}O$ nanoparticles. To obtain the bandgap values, the linear part of the curve was extrapolated to $[F(R)*E]^2 = 0$.

(3.23 eV), pronounced shift to lower energies in the bandgap values of Al-doped ZnO nanopowders was evidenced (Fig. 3, Table 2). Both trends of lowering [46] and increasing [27,30] bandgap energy can be found in the literature. This behaviour is proposed to be a result of a specific structure of prepared $Al_xZn_{1-x}O$, which is caused by different conditions of the reaction procedure. Moreover, the estimation of the bandgap energy may be influenced by the evaluation method. The use of DRUV–Vis data is more sensitive for the band edge changes than the use of UV–Vis absorption measured on colloidal samples. The difference between a dry sample in air and particles dispersed in a liquid with a higher refraction index may play a role as well. A plausible explanation of the observed feature is the distortion of the conductive band structure by the formation of new shallow states and partial filling of the conduction band [47].

Room temperature photoluminescence spectra (Fig. 4) were measured with the use of laser source with excitation wavelength 332.2 nm. The PL spectra illustrated on the left in Fig. 4, show that the PL intensity is increasing with the content of Al dopant. At the same time, a shift of UV emission PL peak toward lower wavelength is observed.

The energy of emission maximum shifts from 377 nm (3.29 eV) for neat ZnO to 367 nm (3.38 eV) for Al10ZnO. Surprisingly, the energy of this transition is larger than the bandgap estimated from the Tauc plot. In this region, many emission origin mechanisms are possible. Radiative recombinations from zinc vacancies, donor-bound excitonic (DBE)

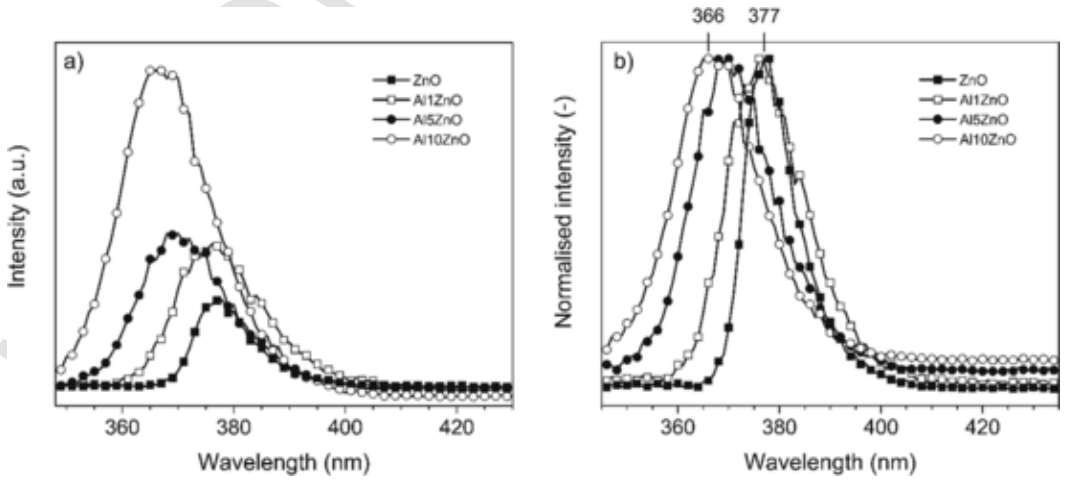

Fig. 4. a) Room temperature PL spectra of $Al_xZn_{1-x}O$ nanodispersions compared with pure ZnO nanocolloid. b) The same spectra as in the left graph normalised. Laser with the wavelength 332 nm was used as an excitation source.

emission, electron-hole recombination, free exciton recombination, free-to-bound transition, surface-bound ionised acceptor-exciton complexes, donor–acceptor pair transition, exciton–exciton collision process are considered [48]. The energy of the excitation laser beam 332 nm (3.74 eV) is sufficient to pump the system for all these transitions as indicated by the arrow in Fig. 3a. Despite the decrease of bandgap energies with increasing doping, the emission maxima exhibit the hypsochromic shift implying thus a complex change of radiative deexcitation channels in the material rather than just the formation of additional new dopant levels. Eventual filling of the lowest states in the conduction band of ZnO by electrons from the dopant may affect the relaxation of excitons which results to the higher energy of radiative recombination transition (Burstein-Moss shift) [47].

3.2. PL study of polymers/$Al_xZn_{1-x}O$ layers

UV–Vis absorption spectra (see Fig. S4 in the Supplement) were measured to confirm the absorption maximum wavelength ($\lambda_{A,max}$) of prepared thin layers. Indeed, the addition of nanofillers did not alter the spectra of used polymers significantly. Hence, the $\lambda_{A,max}$ was used as excitation wavelength for PL experiments with larger information depth. Fig. 5**a** represents the room temperature PL spectra of pure MEH-PPV, MEH-PPV/ZnO, and MEH-PPV/$Al_xZn_{1-x}O$ composite films with different Al concentration (x = 0.01, 0.05, 0.10) measured with excitation light wavelength 515 nm. As mentioned previously, the concentration of particles was 50 wt%, i.e. 15 vol% in prepared films. The wavelength range of emission from 560 nm to 800 nm is mainly due to the conductive polymer MEH-PPV. The incorporation of nanoparticles influences the intensity ratio of the 0–0/0–1 emission (at λ_{em} 595 nm/646 nm), which testifies structural changes in the cast nanocomposite thin film. The changes favour the interchain interaction over the intra-molecular one if nanoparticles are added. In other words, the formation of H-aggregates is more favoured than the formation of J-aggregates. Such mutual interplay of these two aggregation modes has already been demonstrated for some other conductive polymers [49,50]. It enhances strongly the exciton diffusion length, which has a direct effect on the performance of any electronic device based on MEH-PPV due to its straightforward relation to the charge carrier mobility [51]. The room temperature PL spectra of F8BT samples are introduced in Fig. 5b. The same phenomena of the changing intensity ratio of the 0–0/0–1 emission (at λ_{em} 540 nm/575 nm) are observed for F8BT nanocomposite films. Similarly, to MEH-PPV, the formation of H-aggregates is favoured for F8BT after the addition of the nanoparticles.

Note, the incorporation of undoped ZnO nanoparticle into both polymers resulted in a decrease in PL emission intensity of the thin films. On the other hand, the Al-doped ZnO incorporated into MEH-PPV and F8BT polymer matrix yield an increase in photoluminescence intensities in the whole emission interval compared to the PL emission of the undoped ZnO nanocomposite thin-films. This result already implies that the Al-doping of zinc oxide filler in the nanocomposite emissive layer used in PLEDs shall be a promising approach to enhance their performance. In the case of F8BT, the trend is not clear as observed for MEH-PPV, but the highest doping level in ZnO nanoparticle filler provides PL emission intensity reasonably exceeding PL emission intensity of the neat F8BT film.

3.3. The ER-EIS of neat polymers and polymers/nanoparticle composite layers

The electronic structure in terms of density of states (DOS) function, *g(E)*, was measured in both conjugated polymers based thin layers, including the deep states, which are crucial for recombination, and the shallow HOMO (highest occupied molecular orbital) and LUMO (lowest unoccupied molecular orbital) states, which are essential for charge transport. The DOS axis recalculated from the measured resistance, R_{ct}, using Eq. (2) taking into account the concentration at the HOMO and LUMO in the order of 10^{20} $cm^{-3}eV^{-1}$ [52].

Presented DOS spectra (Fig. 6) imply hopping charge transport via the Gaussian distributed localised states to be the predominant transport path. It can be clearly seen that the incorporation of nanoparticles into the polymer matrices influenced the density of states in the bandgap in comparison with neat polymers.

In the case of nanocomposite prepared by incorporation of ZnO into MEH-PPV, the DOS is roughly half order of magnitude higher than neat MEH-PPV. This increase is observed over the whole width of the bandgap. It can be interpreted as a general increase of structural disorder in the polymer matrix, which should result in a decrease of luminescence intensity. Indeed, the decrease of luminescence efficiency was observed for undoped MEH-PPV/ZnO nanocomposite thin films (Fig. 5a). In the case of Al-doped ZnO, the density of deep states near HOMO of the polymer is decreased even in comparison with the neat MEH-PPV film. The increase of DOS nearby LUMO is due to the increase of the n-doping character of the nanoparticles in comparison with the MEH-PPV polymer. Explanation of this phenomenon due to the filling of the traps is more likely than a (highly improbable) increase of conformational order of the polymer chains due to the presence of nanoparticles. The first one of the two explanations are supported by the observed increase of luminescence intensity from the MEH-PPV/Al-doped ZnO thin films.

A similar situation occurs in the case of F8BT. The addition of ZnO nanoparticles introduces the new deep states into the middle of the bandgap with the maximum population at about −4.5 eV. This can be interpreted as in case of MEH-PPV as a structural disorder in the polymer matrix. Moreover, the steepness of the HOMO band is decreased

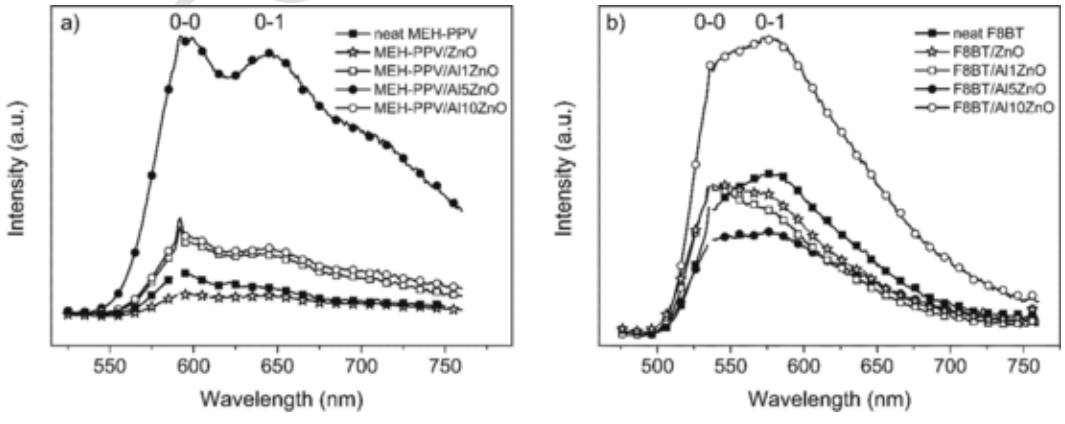

Fig. 5. Photoluminescence spectra of thin films based on a) MEH-PPV, λ_{exc} = 515 nm and b) F8BT, λ_{exc} = 467 nm.

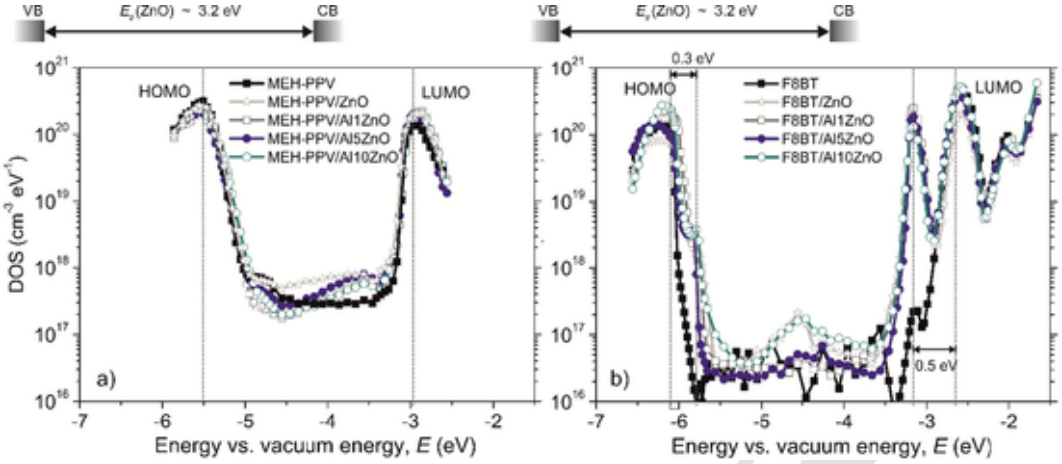

Fig. 6. ER-EIS spectra and dependences of DOS function; a) MEH-PPV based thin films and b) F8BT based thin films. The energies of valence and conduction bands of ZnO is shown in the upper parts of the graphs. (The same scales on *x*- and *y*-axe are set intentionally to enable the comparison easier.)

and new states were induced 0.3 eV above the HOMO energy level (−6.1 eV). Since positive doping by the nanoparticles is not expected, the state population may be caused by a conformational change of the polymer chain similarly as it was observed for poly(9,9-dioctylfluorene) [53]. There are shallow states present 0.5 eV below the LUMO (−2.65 eV) in the pristine polymer film. The introduction of the nanoparticles generated an enormous increase of the population of the states at this energy (at about −3.15 eV) practically achieving the density of the neat polymer LUMO. Since transport bandgap structure is mapped by the ER-EIS, it can be expected, the new prevailing electron transfer channel was created. The exciton binding energy in the neat polymer film is relatively high, i.e. ca 1.2 eV as calculated from the difference between HOMO and LUMO estimated by ER-EIS (3.5 eV in Fig. 6) and the energy of the 0–0 radiative transition (540 nm ~ 2.3 eV in the PL spectra in Fig. 5) [54,55]. It is in accordance with the known localized nature of the electron in the LUMO of F8BT, which is unique and very different from other conjugated polymers. Nevertheless, the introduction of the nanoparticles decreases the exciton binding energy by 0.5 eV independently on the aluminium doping level (see Fig. 6). Thus, it is most likely the introduction of polymer chain packing disorder that may deteriorate the alternating structure of adjacent BT and F8 mer units in neighboring polymer chains [56]. Such structural feature should enhance the interchain electron transfer (hopping) through the population of states at ca −3.15 eV and improve the charge carrier balance in the nanocomposite F8BT polymer thin film when operated in a PLED device.

3.4. Electroluminescence and performance of PLED devices

The doped nanoparticle material $Al_{0.1}Zn_{1-0.1}O$ was chosen as the most promising candidate among synthesised fillers for the fabrication of PLED devices, based on PL and ER-EIS investigation of its nanocomposites in MEH-PPV and F8BT polymer matrices.

The current–voltage (I-V) characteristics of prepared orange MEH-PPV based PLEDs are presented in Fig. 7**a**. The dependences of the luminance on the power in the sample are in Fig. 7c. The luminance is recorded as the photodiode current (PD) from the detecting diode collecting directly the light emitted from the tested specimen. The I-V curves zoomed in the graph inset in Fig. 7a characteristically display a decrease in the opening bias with polymer-nanoparticle composite compared to the neat polymer-based device. The opening bias of neat MEH-PPV device is around 5.1 V, and that of MEH-PPV/ZnO is approximately 4.1 V. PLED devices with aluminium-doped ZnO nanoparticles exhibited the opening bias about 2.4 V, which is close to the value 2.5 eV of the transport bandgap estimated by ER-EIS. This seemingly contradictory result is explained by the Auger-like energy upconversion mechanism, which enables electroluminescence at sub-bandgap voltages [57].

The superiority of nanocomposite diodes over the neat MEH-PPV one is manifested by enhanced luminance at higher input powers (Fig. 7c). The nanocomposite diodes provide similar emission intensity when powered below 0.2 W, which is the critical maximum for a neat MEH-PPV diode. The nanocomposite diode with undoped ZnO can be operated up to ca 0.3 W while the one with Al-doped ZnO nanoparticles can be operated up to ca 0.7 W with nearly ten times higher luminance than the maximum achievable for the neat MEH-PPV diode. Based on this result, a longer lifetime can be predicted for the Al-doped ZnO nanocomposite diodes.

The electroluminescence spectra are plotted in the graph shown in Fig. 8**a**. A significant increase in EL peak maxima intensity with Al-doped nanoparticles was observed. The sample MEH-PPV/Al10ZnO has four times higher EL intensity than the sample containing undoped ZnO, and 15 times higher than the neat MEH-PPV reference when forwarded up to 10 V. According to the typical shape of the emission spectra, the electroluminescence is a result of radiative recombination between electrons and holes in MEH-PPV polymer matrix where the 0–0 transition path is mainly preferred. In contrast, 0–1 vibronic relaxation path is mostly suppressed.

Current-voltage characteristics of prepared yellow F8BT PLEDs are presented in Fig. 7b, the dependences of PD current of detecting diode on the sample power input are shown in Fig. 7d. As in the case of orange diodes, the decrease in opening bias in comparison with the neat polymer-based device was confirmed for nanoparticle addition. The opening bias of the neat F8BT device is around 4.9 V, that of F8BT/ZnO is approximately 2.8 V, and that of F8BT/Al10ZnO is 4.8 V. The transport gap estimated by ER-EIS is 3.5 eV for the neat F8BT. The difference between opening bias and the transport gap can be explained by the sub-bandgap voltage electroluminescence [57]. The PD current is much lower than that of the neat F8BT reference over the whole operation power range. Nevertheless, the ending point in both PD curves shows slightly higher luminance for the nanocomposite PLED. Both were recorded at 10 V of powering voltage, see also the ending point of the I-V curves in Fig. 7b. Altogether, the poor luminance efficiency of this nanocomposite diode could be explained by a high leakage current. Nevertheless, in the case of doped ZnO nanoparticles, the behaviour differs in comparison with pure ZnO. In the composite F8BT/Al10ZnO layer, the opening bias increases again. However, the PD current grows much faster with power input compared to the neat polymer reference. The F8BT/Al10ZnO diode can be optimally operated at 0.25 W with ten times higher luminance than observed for the neat F8BT diode at

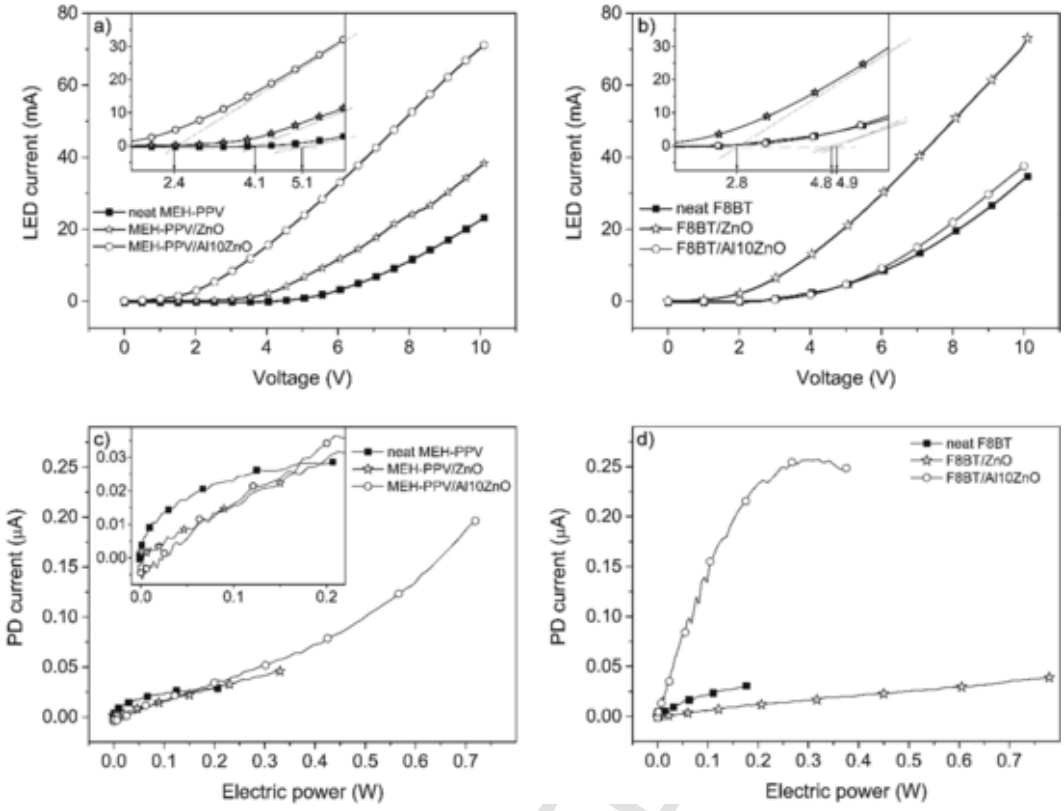

Fig. 7. I-V characteristics of prepared diodes a) and b), and dependences of measured PD current on the power input to the diodes c) and d).

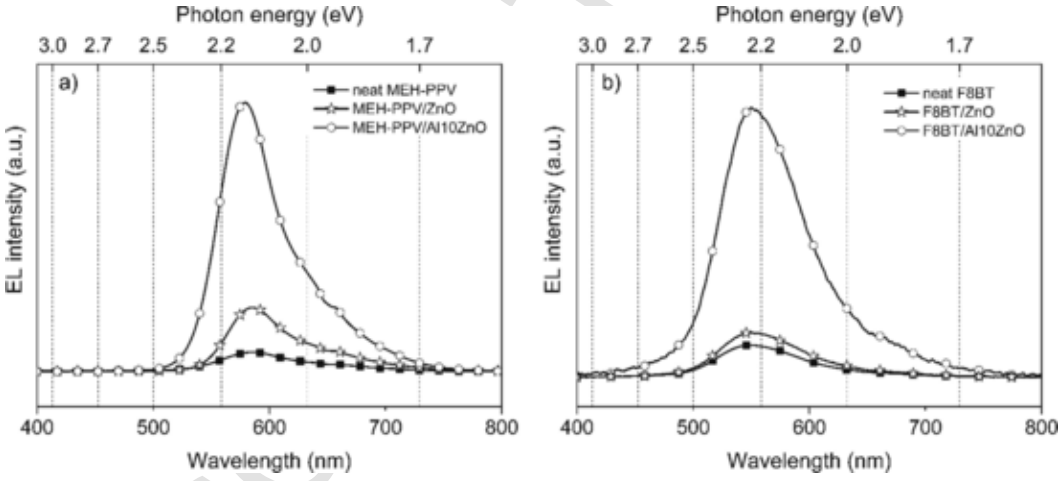

Fig. 8. Electroluminescence spectra of prepared diodes based on a) MEH-PPV and b) F8BT matrices, operated at 10 V.

0.18 W. Utilization of the ZnO nanoparticles with the highest Al doping concentration in the nanoparticle-polymer bulk heterostructure nanocomposite yielded the best performing diode among all tested devices.

The electroluminescence spectra of the F8BT based devices are plotted in the graph in Fig. 8b. Also here, the 0–0 transition in F8BT polymer chains evidently prevails as the dominant radiative recombination mechanism.

The chromaticity of the light emitted by the prepared diodes is depicted in trichromatic diagram CIE 1931 2° in Fig. 9 to compare the appearance of the prepared light sources.

In the case of MEH-PPV based diodes, it seems that the addition of nanoparticles shifts the chromaticity to the spectral locus, and the emitted light from diodes with nanocomposite layers appear monochromatic. In the case of F8BT based diodes, a similar shift is also observed, but the points are not located directly on the monochromatic locus. In Fig. 10, the photographs of prepared diodes are shown to visualise how the emitted lights look like in a real situation.

To analyse and discuss the performance of prepared devices, their parameters should also be expressed in terms of luminance and current efficiency. Such an approach enables comparing the performance of prepared PLEDs with data reported once. Performance indicators for all prepared and tested samples are summarized in Table 3. It should be noted that the used method involves measurement with the integrating sphere only, which does not allow to measure the angular dependency of the luminous intensity. Hence, the value of the apex angle is fixed at 180°. Therefore, the method provides the lowest possible (and most sceptic) estimate of the device luminance. Nevertheless, within the pre-

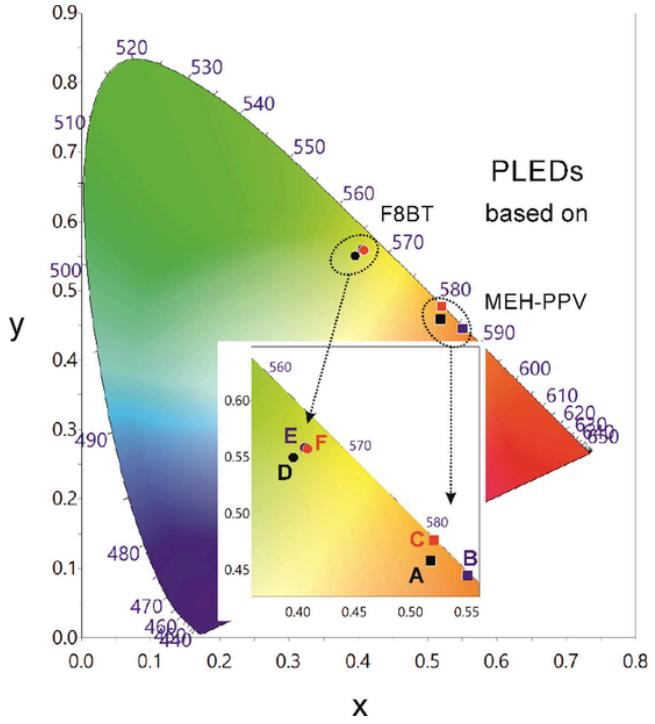

Fig. 9. Final color of prepared diodes depicted in trichromatic diagram CIE 1931 2°.

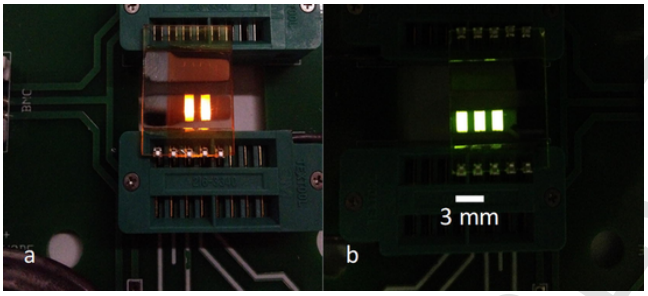

Fig. 10. Examples of best-performing diodes consisted of a – MEH-PPV/Al10ZnO and b – F8BT/Al10ZnO. The scale bar in the right panel applies for both images.

Table 3
Comparison of parameters of prepared polymer LEDs operated at the forward bias 10 V.

Sample type	Luminance, L_{vPLED} [cd/m^2]	Current efficiency, CE [cd/A]	Current density, J [A/m^2]	Performance ratio
neat MEH-PPV	1 900.00	0.37	5 200.00	1.0
neat F8BT	4 600.00	0.60	7 600.00	1.0
MEH-PPV/ZnO	5 100.00	0.63	8 100.00	2.7
F8BT/ZnO	6 700.00	0.38	18 000.00	1.5
MEH-PPV/ Al10ZnO	21 000.00	1.3	16 000.00	10.9
F8BT/Al10ZnO	38 000.00	4.6	8 200.00	8.3

pared sample set, the individual devices can be ranked easily using the performance ratio, which is a value describing the luminance improvement of devices with active layer from nanocomposite in comparison with devices based on neat polymer active layer. Addition of any ZnO nanoparticles always resulted in performance improvement. Moreover, the use of Al10ZnO nanoparticles as fillers for the nanocomposite emissive layer allowed fabrication of diodes with the current efficiency exceeding at least the value of 1 cd/A for MEH-PPV/Al10ZnO and 4 cd/A for F8BT/Al10ZnO. Numerous studies have already reported current efficiency in order of units or tens of cd/A for F8BT and MEH-PPV based diodes with precise and elaborated multilayer structure using vacuum-based technology [58–60]. Nevertheless, the performances presented in this work were achieved with the simplest possible device structure and fabrication technology, thus, testifying to the superiority of the nanoparticle-polymer nanocomposite bulk heterostructure for the emissive layer. Achieved luminances were one order of magnitude higher than the results presented in the literature [61].

3.5. Discussion of the band structure of prepared PLED devices

As already stated above, the radiative recombination occurs always on the polymer chain preferring the 0–0 transition in EL spectra of all studied PLEDs. The increased current density and enhanced EL intensity by the incorporation of ZnO nanofillers may be ascribed partly to the enhancement of charge injection and transport and associated improved balance of the charge carriers polarity. The role of ZnO nanoparticulate fillers in emissive layers of prepared PLEDs shall be understood in terms of the energy-level diagrams of the devices. The DOS mapping performed by ER-EIS in section 3.3. yielded transport gaps unlike all the literature reporting optical gaps and band positions. Therefore, the following discussion and developed schemes correspond to the values taken from the literature [57,62–66] and obtained experimentally by optical spectroscopies, while the features detected by the ER-EIS in the bandgap are located on the energy scale according to their relative positions related to LUMO or HOMO of the respective polymers.

Fig. 11 illustrates the standard band structure of prepared neat MEH-PPV (a) and F8BT (b) devices.

In both cases, the electrons are injected directly from the magnesium cathode to the LUMO of the polymers as illustrated by the path **e1**. The electrons must overcome the energy barrier which is almost two times higher for MEH-PPV than for F8BT. The hole injection from ITO anode to the HOMO of the polymer is facilitated by a cascade of **h1** and **h2** pathways through a standard PEDOT:PSS buffer layer. Owing to the typical hole conductivity of MEH-PPV as well as the energy barriers in prepared devices, the charge carrier balance is highly distorted in the device based on this polymer. Due to the better-balanced charge carrier concentrations of the F8BT and more favourable energy barriers in the **e1** and **h2** pathways, the neat F8BT based PLED is more efficient than the neat MEH-PPV one [7,67].

It was demonstrated that the addition of the undoped ZnO nanoparticles to the emissive layer can improve the current density and electroluminescence intensity of prepared PLEDs. The nanoparticles have an electron type of conductivity. As such, they may improve electron injection into the emissive layer as their incorporation increases of the p-n interface area between the polymer and semiconductor phase in the bulk heterostructure which shall be especially important for the almost

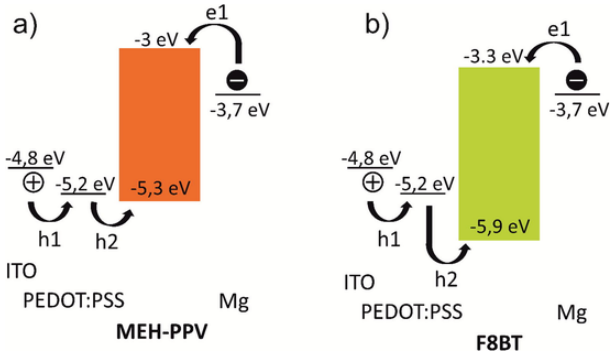

Fig. 11. Schematic energy level diagram of a) MEH-PPV and b) F8BT devices.

purely p-type polymer MEH-PPV [35,68,69]. The connection between polymer chains adjacent to the same ZnO nanoparticle with enhanced electron conductivity may also increase charge carriers transport in the nanocomposite layers. Thus, the current would not be limited by hopping of the charge carriers between individual polymer chains only. According to the ER-EIS analysis, the performance of prepared PLED can be influenced by the introduction of ZnO nanoparticles principally in a twofold manner.

First, the nanoparticles can directly improve the electron injection from the Mg cathode to LUMO of the polymer via a sequence of **e2** and **e3** pathways, while **e1** remains still possible as illustrated in Fig. 12.

The position of the conduction band of ZnO versus the Fermi level of Mg enhances electron injection through **e2** for all devices in the same way. The energy barrier between involved energy levels in **e3** is much smaller for F8BT/ZnO (Fig. 12 b) than for MEH-PPV/ZnO (Fig. 12 a). Therefore, the effect shall be more pronounced for the former case. Nevertheless, the **e3** energy barrier can be overcome by the Auger-like energy upconversion mechanism even at sub-bandgap voltages. Each electron upconversion event is realised at the expense of futile recombination of another electron and a hole [57]. This relatively subtle effect may be more important for MEH-PPV/ZnO material. On the other hand, the hole blocking effect **h3** of ZnO is expected for both polymer matrices due to its high energy barrier. Again here, its contribution may be more important in case of the MEH-PPV since it is a hole transporting polymer mainly and it combines with the **e1** and **e3** pathway barriers which are higher than for F8BT.

The second effect of the ZnO nanoparticle addition is indirect. Incorporation of the nanofiller influences structural order of the polymer matrix inducing thus new energy states in the bandgap of the polymer. For MEH-PPV/ZnO, only the general increase of structural disorder in the polymer matrix was observed as illustrated in Fig. 12 a) by plotting a schematic distribution of newly created DOS over the whole width of the bandgap. The indirect effect is much more pronounced in case of the F8BT/ZnO (see Fig. 12 b). Deterioration of the alternating structure of adjacent BT and F8 mer units in neighbouring F8BT chains changes the electronic structure of the material [56]. Our ER-EIS analysis revealed that the structural disorder resulted in a new prevailing electron transfer channel located about 0.5 eV below LUMO of the neat F8BT. The band is relatively narrow (ca 0.3 eV), as can be seen in Fig. 6 b. This alternative LUMO energy level formed in disordered F8BT practically aligns with the Fermi level of the cathode (**e1** pathway) and reduces the energy barrier for the **e3** pathway significantly too. In Fig. 12 b, an increase in density of deep states is observable in the middle of the bandgap of the F8BT which may also be due to the disorder increase [56]. Moreover, the new states induced 0.3 eV above the HOMO of F8BT in F8BT/ZnO may influence the hole injection and transport as well as provide an alternative and less energetically demanding pathway **h2′** for **h2**.

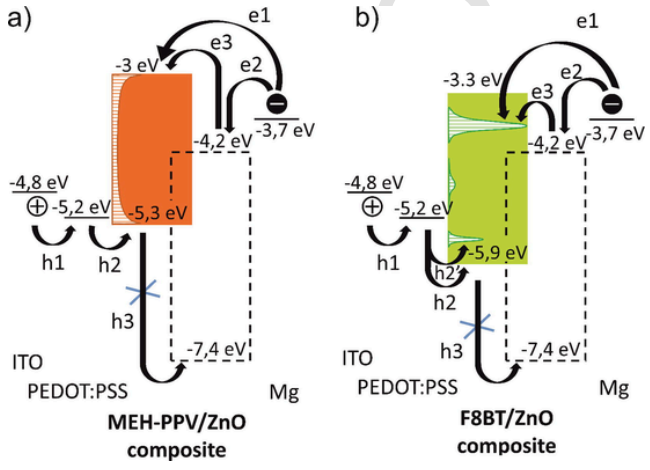

Fig. 12. Schematic energy level diagram of a) MEH-PPV/ZnO and b) F8BT/ZnO devices.

The n-type doping of ZnO nanoparticles by Al resulted in new states both below and in its conduction band as schematically depicted in Fig. 13. The edge of the conduction band of the doped ZnO became more blurred rather than shifted as indicated by the optical spectroscopies. The width of the distribution of states around the conduction band edge of the ZnO is only roughly guessed from the change of the absorption spectrum in Fig. 3 to be about 0.4 to 0.5 eV.

Thus, more energy levels are provided for alignment of the conduction bands with the Fermi level of the cathode. Moreover, the dispersion of energy states in unoccupied bands both in the polymer as well as in the semiconductor nanoparticles may overlap and reduce the barriers for hopping, which may cause an overall increase in carrier density. Unlike promoted electron pathways **e1**, **e2**, and **e3**, the barrier for **h3** remains unchanged by the n-doping of the nanoparticles and contributes positively to the charge carrier transfer balance in the devices.

Besides the same indirect effects as in the case of undoped nanoparticles, the addition of Al-doped ZnO nanoparticles significantly alters the electronic structure of deep states in the bandgap MEH-PPV while the structure of F8BT seems to be affected in the very same way as in case of the F8BT/ZnO nanocomposite. MEH-PPV is almost purely a hole transporting polymer and addition of Al-doped ZnO increased DOS (local maximum at ca −3.5 eV) nearby LUMO by n-doping while the DOS (local minimum ca −4.5 eV) near HOMO is decreased in comparison with the neat MEH-PPV film most likely by filling of the traps (see Fig. 13 a). The inflexion point of this deep state distribution is found around −4 eV in Fig. 6 a) and the width of this feature testifies for a similar wide distribution of states around the conduction band edge of the doped ZnO. As a result, higher efficacy of the Al-doped ZnO nanocomposite based PLEDs in comparison with those with emissive layers filled by undoped ZnO nanoparticles was observed.

To summarize, observed properties of ZnO and Al-doped ZnO nanoparticle nanocomposites used as emissive layers can be rationalized in terms of the energy-level diagrams of prepared PLEDs and give a conclusive picture of their effects resulting to the enhanced performance of tested sample devices. The ER-EIS spectroscopy offers direct insight into the electronic structure of the thin films. Thus, it is a powerful methodology complementing contemporary analytical approaches used for the fabrication of high-efficiency organic light-emitting diodes [13].

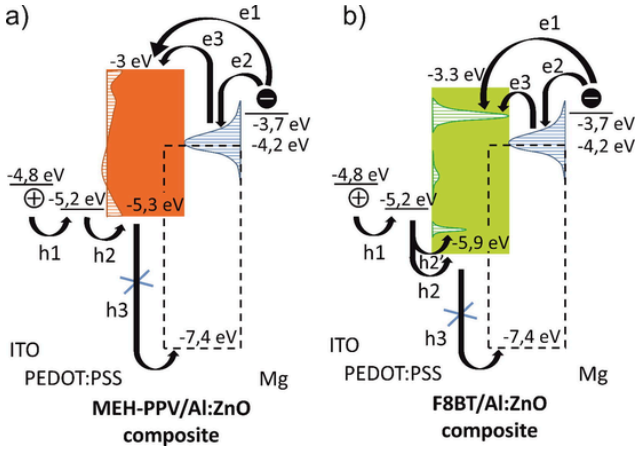

Fig. 13. Schematic energy level diagram of a) MEH-PPV/Al:ZnO and b) F8BT/Al:ZnO devices.

4. Conclusions

Our work presented the facile microwave-assisted synthesis of Al-doped ZnO nanoparticles, which have been successfully incorporated into the polymer matrices to prepare nanocomposite thin films by spin coating. The photoluminescence spectra of the nanocomposites testify to the influence of nanoparticle incorporation on the development of the polymer structure of the thin films which was revealed by the energy-resolved electrochemical impedance spectroscopy (ER-EIS). These films were used as active layers in the polymer light-emitting diodes.

The PLED devices were fabricated with the use of MEH-PPV and F8BT polymers in a simple manner with easy control of processing conditions. No ETL layer, no oxidising metal, only a nanocomposite active layer cast in one step is used. The incorporation of ZnO nanoparticles as fillers in the nanoparticle-polymer nanocomposite bulk heterostructure for the emissive layer improved the performance of the prepared PLEDs in all cases. The electroluminescence spectrum comprised only the polymer matrix emission with increased intensity attributed to the 0–0 vibronic transition. Besides an increase in luminance, such change shifts the emission closer to monochromaticity. Moreover, n-type doping of ZnO nanoparticles by Al greatly (10 times) enhances the electroluminescence and luminance of the nanocomposite PLED devices, even in contrast to neat polymer and polymer/ZnO-based nanocomposites (from 1 900 to 20 700 cd/m^2 in case of MEH-PPV and from 4 600 to 38 000 cd/m^2 in case of F8BT).

The effect of nanoparticle incorporation to the emissive layer is twofold:

1. The direct involvement of the ZnO nanoparticles into the charge carrier injection and transport processes. The electroluminescence is enhanced due partly to promoting electron injection of electrons from the cathode to the layer (**e2**) and their transport through the layer and injection onto polymer chains in the bulk heterostructure interface (**e2**), and due partly to impeding the hole transport (**h3**). Aluminium doping of the ZnO nanoparticles improves then significantly the pathways for electron transport (both **e2** and **e3**), while the blocking barrier remains unaffected. This should positively contribute to the charge carrier balance. It was also found that Al-doped ZnO nanoparticles fill the traps above HOMO and increase the density of states below LUMO in MEH-PPV polymer as they may be n-doping to MEH-PPV. In the case of F8BT, the increased dispersion of energy states below and above the edge of ZnO due to aluminium doping contributes to better alignment of the electron injection and transport levels (bands) in the active layer as they may overlap more reducing thus the barriers for hopping.
2. The second kind of effects is indirect and unspecific to doping by aluminium. The addition of nanoparticles increases the disorder in the polymer structure, which impacts on the electronic structure of the polymer matrix itself. The disorder increase was manifested only as an overall increase of DOS in the bandgap in MEH-PPV. On the other hand, the effect on F8BT was dramatic. A new transport-level 0.5 eV below the original LUMO level with nearly the same DOS as a result of the deterioration of the alternating structure of adjacent BT and F8 mer units in neighboring F8BT chains. Notably, this new electron transport level corresponds to the Fermi level of the Mg cathode, improving thus the electron injection (**e1**). Moreover, a possible alternative pathway for hole transport (**h2′**) with a lower energy barrier yet of a lower density of states created 0.3 eV above the HOMO of the polymer as well.

Declaration of Competing Interest

The authors declare that they have no known competing financial interests or personal relationships that could have appeared to influence the work reported in this paper.

Acknowledgments

This work was funded by the Ministry of Education, Youth and Sports of the Czech Republic—Program NPU I (LO1504). Further, this work was supported by the Ministry of Education, Youth and Sports of the Czech Republic – DKRVO (RP/CPS/2020/006). The authors T.J. and I.K. specifically acknowledge funding by the Internal Grant Agency of Tomas Bata University in Zlín, grant no. IGA/CPS/2019/007 and no. IGA/CPS/2020/003. This article was also written with the support of Operational Program Research and Development for Innovations co-funded by the European Regional Development Fund and the national budget of Czech Republic, within the framework of project CPS - strengthening research capacity (reg. number: CZ.1.05/2.1.00/19.0409). This work was performed during the implementation of the project Building-up Centre for advanced materials application of the Slovak Academy of Sciences, ITMS project code 313021T081 supported by the Research & Innovation Operational Programme funded by the ERDF.

Appendix A. Supplementary material

Supplementary data to this article can be found online at https://doi.org/10.1016/j.matdes.2021.109738.

References

[1] C. Adachi, Jpn. J. Appl. Phys. (2014) 53, doi:10.7567/JJAP.53.060101.
[2] R.M. Overney, C. Buenviaje, R. Luginbuhl, F. Dinelli, J. Therm. Anal. Calorim. 59 (2000) 205.
[3] S.R. Forrest, Nature 428 (2004) 911.
[4] S.V. Kunz, C.M. Cole, A. Welle, P.E. Shaw, P. Sonar, N.-P. Thoebes, T. Baumann, S.D. Yambem, E. Blasco, J.P. Blinco, C. Barner-Kowollik, Macromolecules 52 (2019) acs. macromol.9b02030.
[5] V.M. Korshunov, T.N. Chmovzh, E.A. Knyazeva, I.V. Taydakov, L.V. Mikhalchenko, E.A. Varaksina, R.S. Saifutyarov, I.C. Avetissov, O.A. Rakitin, Chem. Commun. 55 (2019) 13354.
[6] T. Zhang, J. Sun, X. Liao, M. Hou, W. Chen, J. Li, H. Wang, L. Li, Dye. Pigment. 139 (2017) 611.
[7] U. Giovanella, M. Pasini, C. Botta, Organic Light-Emitting Diodes (OLEDs): Working Principles and Device Technology, 2016
[8] J.H. Burroughes, D.D.C. Bradley, A.R. Brown, R.N. Marks, K. Mackay, R.H. Friend, P.L. Burns, A.B. Holmes, Nature 347 (1990) 539.
[9] J.S. Salafsky, Phys. Rev. B - Condens. Matter Mater. Phys. 59 (1999) 10885.
[10] N.A. Anderson, E. Hao, X. Ai, G. Hastings, T. Lian, Chem. Phys. Lett. 347 (2001) 304.
[11] A. Petrella, M. Tamborra, M.L. Curri, P. Cosma, M. Striccoli, P.D. Cozzoli, A. Agostiano, J. Phys. Chem. B 109 (2005) 1554.
[12] H. Yan, S. Limbu, X. Wang, J. Nightingale, I. Hamilton, J. Wade, S. Kwon, K. Lee, J.S. Kim, Adv. Funct. Mater. (2019) 29, doi:10.1002/adfm.201904092.
[13] J.H. Jou, S. Kumar, A. Agrawal, T.H. Li, S. Sahoo, J. Mater. Chem. C 3 (2015) 2974.
[14] M. Arvand, A.A. Mirroshandel, Food Chem. 280 (2019) 115.
[15] J.W. Han, C.W. Joo, J. Lee, D.J. Lee, J. Kang, S. Yu, W.J. Sung, N.S. Cho, Y.H. Kim, Sci. Technol. Adv. Mater. 20 (2019) 35.
[16] Y. Sun, W. Wang, H. Zhang, Q. Su, J. Wei, P. Liu, S. Chen, S. Zhang, ACS Appl. Mater. Interfaces 10 (2018) 18902.
[17] Y. Azizian-Kalandaragh, U. Aydemir, Ş. Altindal, J. Electron. Mater. 43 (2014) 1226.
[18] G. Jiang, A.S. Susha, A.A. Lutich, F.D. Stefani, J. Feldmann, A.L. Rogach, ACS Nano 3 (2009) 4127.
[19] C. Sekine, Y. Tsubata, T. Yamada, M. Kitano, S. Doi, Sci. Technol. Adv. Mater. (2014) 15, doi:10.1088/1468-6996/15/3/034203.
[20] R. Kaçar, S.P. Mucur, F. Yldldz, S. Dabak, E. Tekin, Appl. Phys. Lett. 112 (2018), doi:10.1063/1.5015955.
[21] C.F. Klingshirn, ChemPhysChem 8 (2007) 782.
[22] Ü. Özgür, Y.I. Alivov, C. Liu, A. Teke, M.A. Reshchikov, S. Doğan, V. Avrutin, S.J. Cho, H. Morko, J. Appl. Phys. 98 (2005) 1.
[23] K. Tang, S.L. Gu, J.D. Ye, S.M. Zhu, R. Zhang, Y.D. Zheng, Chinese Phys. B (2017) 26, doi:10.1088/1674-1056/26/4/047702.
[24] T.C. Bharat, Shubham, S. Mondal, H.S. Gupta, P.K. Singh, A.K. Das, Mater. Today Proc. 11 (2019) 767.

[25] F. Maldonado, A. Stashans, J. Phys. Chem. Solids 71 (2010) 784.
[26] W. Ma, Y. Luo, L. Nian, J. Wang, X. Wen, L. Liu, M. Hanif, Z. Xie, Y. Ma, ACS Appl. Mater. Interfaces 10 (2018) 10513.
[27] N. Kumar, A. Srivastava, Opto-electronics Rev. 26 (2018) 1.
[28] H. Kim, C.M. Gilmore, J.S. Horwitz, A. Piqué, H. Murata, G.P. Kushto, R. Schlaf, Z.H. Kafafi, D.B. Chrisey, Appl. Phys. Lett. 76 (2000) 259.
[29] X. Jiang, F.L. Wong, M.K. Fung, S.T. Lee, Appl. Phys. Lett. 2003 (1875) 83.
[30] R. Buonsanti, A. Llordes, S. Aloni, B.A. Helms, D.J. Milliron, Nano Lett. 11 (2011) 4706.
[31] I. Bilecka, P. Elser, M. Niederberger, ACS Nano 3 (2009) 467.
[32] E. Hammarberg, A. Prodi-Schwab, C. Feldmann, J. Colloid Interface Sci. 334 (2009) 29.
[33] D. Skoda, P. Urbanek, J. Sevcik, L. Munster, V. Nadazdy, D.A. Cullen, P. Bazant, J. Antos, I. Kuritka, Org. Electron. Phys., Mater. Appl. 59 (2018), doi:10.1016/j.orgel.2018.05.037.
[34] T. Jamatia, D. Skoda, P. Urbanek, J. Sevcik, J. Maslik, L. Munster, L. Kalina, I. Kuritka, J. Mater. Sci. Mater. Electron. 30 (2019) 11269.
[35] D. Skoda, P. Urbanek, J. Sevcik, L. Munster, J. Antos, I. Kuritka, Mater. Sci. Eng. B Solid-State Mater. Adv. Technol. 232–235 (2018) 22.
[36] M. Takada, T. Mayumi, T. Nagase, T. Kobayashi, H. Naito, Appl. Phys. Lett. 114 (2019) 123301.
[37] O.P.M. Gaudin, I.D.W. Samuel, S. Amriou, P.L. Burn, J. Appl. Phys. 127 (2020) 093101.
[38] A. Dey, D. Kabra, ACS Appl. Mater. Interfaces 10 (2018) 38287.
[39] V. Nadazdy, F. Schauer, K. Gmucova, Appl. Phys. Lett. 105 (2014), doi:10.1063/1.4898068.
[40] F. Schauer, V. Nádazdy, K. Gmucová, J. Appl. Phys. 123 (2018), doi:10.1063/1.5008830.
[41] F. Schauer, J. Appl. Phys. 128 (2020) 150902.
[42] M. Sabzi, S.M. Far, S.M. Dezfuli, Int. J. Miner. Metall. Mater. (2018) 25, doi:10.1007/s12613-018-1697-1.
[43] M. Sabzi, S. Mersagh Dezfuli, Int. J. Appl. Ceram. Technol. 2019, 16, 195.
[44] A. Khorsand Zak, W.H. Abd, M.E. Majid, R. Yousefi Abrishami, Solid State Sci. 13 (2011) 251.
[45] A. Wang, T. Chen, S. Lu, Z. Wu, Y. Li, H. Chen, Y. Wang, Nanoscale Res. Lett. (2015) 10, doi:10.1186/s11671-015-0801-y.
[46] M.M. Rahman, M.K.R. Khan, M.R. Islam, M.A. Halim, M. Shahjahan, M.A. Hakim, D.K. Saha, J.U. Khan, J. Mater. Sci. Technol. 28 (2012) 329.
[47] B.E. Sernelius, K.F. Berggren, Z.C. Jin, I. Hamberg, C.G. Granqvist, Phys. Rev. B 37 (1988) 10244.
[48] S. Repp, E. Erdem, Spectrochim. Acta - Part A Mol. Biomol. Spectrosc. 2016, 152, 637.
[49] P. Urbanek, I. Kuritka, J. Lumin. 168 (2015) 261.
[50] P. Urbánek, I. Kuřitka, J. Ševčík, J. Toušková, J. Toušek, V. Nádaždy, P. Nádaždy, K. Végsö, P. Šiffalovič, R. Rutsch, M. Urbánek, Polymer (Guildf). 169 (2019) 243.
[51] P. Urbanek, I. Kuritka, S. Danis, J. Touskova, J. Tousek, Polymer (Guildf). 55 (2014) 4050.
[52] N. Vukmirovic, L.W. Wang, J. Phys. Chem. B 115 (2011) 1792.
[53] X. Shi, V. NádaŽdy, A. Perevedentsev, J.M. Frost, X. Wang, E. Von Hauff, R.C.I. Mackenzie, J. Nelson, Phys. Rev. X 9 (2019) 021038.
[54] C. Deibel, D. MacK, J. Gorenflot, A. Schöll, S. Krause, F. Reinert, D. Rauh, V. Dyakonov, Phys. Rev. B - Condens. Matter Mater. Phys. 81 (2010) 085202.
[55] J.H. Bombile, M.J. Janik, S.T. Milner, Energetics of Exciton Binding and Dissociation in Polythiophenes: A Tight Binding Approach, n.d.
[56] C.L. Donley, J. Zaumseil, J.W. Andreasen, M.M. Nielsen, H. Sirringhaus, R.H. Friend, J.S. Kim, J. Am. Chem. Soc. 127 (2005) 12890.
[57] L. Qian, Y. Zheng, K.R. Choudhury, D. Bera, F. So, J. Xue, P.H. Holloway, Electroluminescence from light-emitting polymer/ZnO nanoparticle heterojunctions at sub-bandgap voltages, Elsevier B.V. (2010).
[58] L.P. Lu, C.E. Finlayson, R.H. Friend, Semicond. Sci. Technol. 29 (2014) 6.
[59] M. Suh, J. Bailey, S.W. Kim, K. Kim, D.J. Yun, Y. Jung, I. Hamilton, N. Chander, X. Wang, D.D.C. Bradley, D.Y. Jeon, J.S. Kim, ACS Appl. Mater. Interfaces 7 (2015) 26566.
[60] B.R. Lee, E.D. Jung, J.S. Park, Y.S. Nam, S.H. Min, B.S. Kim, K.M. Lee, J.R. Jeong, R.H. Friend, J.S. Kim, S.O. Kim, M.H. Song, Nat. Commun. 5 (2014) 1.
[61] D. Moghe, D. Kabra, in Adv. Nanomater. Sol. Cells Light Emit. Diodes, Elsevier, 2019, pp. 343–369.
[62] A. Petrella, M. Tamborra, M.L. Curri, P. Cosma, M. Striccoli, P. Davide Cozzoli, A. Agostiano, 2005, DOI 10.1021/jp046597c.
[63] A.C. Morteani, A.S. Dhoot, J.S. Kim, C. Silva, N.C. Greenham, C. Murphy, E. Moons, S. Ciná, J.H. Burroughes, R.H. Friend, Adv. Mater. 15 (2003) 1708.
[64] M. Willander, O. Nur, J.R. Sadaf, M.I. Qadir, S. Zaman, A. Zainelabdin, N. Bano, I. Hussain, Materials (Basel). 3 (2010) 2643.
[65] S. Janietz, D.D.C. Bradley, M. Grell, C. Giebeler, M. Inbasekaran, E.P. Woo, Appl. Phys. Lett. 73 (1998) 2453.
[66] M.F. Ng, S.L. Sun, R.Q. Zhang, J. Appl. Phys. 97 (2005) 103513.
[67] 1980- editor Inamuddin, R. Boddula editor, M. I. Ahamed editor, A. M. Asiri editor, Eds. , Polymers for Light-Emitting Devices and Displays / Edited by Inamuddin, Rajender Boddula, Mohd Imran Ahamed and Abdullah M. Asiri., Hoboken, NJ : John Wiley & Sons, Inc., 2020., 2020.
[68] A. Petrella, M.L. Curri, M. Striccoli, A. Agostiano, P. Cosma, Thin Solid Films 595 (2015) 157.
[69] J. Toušková, J. Toušek, J. Rohovec, A. Růžička, O. Polonskyi, P. Urbánek, I. Kuřitka, J. Nanoparticle Res. (2014) 16, doi:10.1007/s11051-014-2314-5.